

Tomographic reconstruction of the inclining vortex wind field from the acoustic travel time data between a pair of facing line array

Haiyue Li (1), Akira Yamada (1)

(1)Tokyo University of Agriculture and Technology, 2-24-16 Nakamachi, Koganei, Tokyo, 184-8588, Japan

PACS: 43.35.Yb

Ultrasonic instrumentation and measurement techniques

ABSTRACT

For the monitoring of the strong vortex wind field like a tornado, an acoustic tomographic technique for the reconstruction of two-dimensional vortex air flow profile from the observation of the acoustic travel time data between facing pairs of line array was investigated. When the vortex wind field is inclined with respect to the observation plane, superposition of the axial constant air flow component hampers the estimation of the horizontal vortex air flow fields. For the solution of this problem, a tomographic method for the inclining vortex air flow profile from the single view parallel array observation data has been demonstrated. We assumed that wind field consists of the superposition of the anti-symmetric vortex flow and symmetric vertical axial flow. On this basis, the extraction of the anti-symmetric vortex flow components was presented. Test examinations were carried out using an indoor model equipment with the multi-channel bidirectional ultrasonic transmitter/receiver circuit. It was demonstrated that vortex wind velocity fields could be reconstructed with satisfactory quantitative precision of the vortex maximum velocities and size.

1. INTRODUCTION

A monitoring system for a gust of wind like a tornado is desired such as in railroads or airports. It is not realistic to use an anemometer for this purpose because ordinary anemometers are of fixed observation in situ and large numbers must be needed. Acoustic tomography¹⁻⁴ is expected to be the solution to the problem, since airflow velocity profile can be reconstructed by the calculation on the basis of measurement data of acoustic travel times in the channels between transmitters and receivers. So far, a method has been proposed by the present author by placing acoustic line array elements along the facing sides of the monitoring region^{5,6}. The method was however limited for the non-inclining vortex wind field, which was not practical in real situation. In order to extend the previous method to cover the inclining vortex wind field, superposition of the vertical axial air flow component hampers the reconstruction of the vortex air flow profile. To this end, the target horizontal vortex components are extracted from the superposed axial flow components using the symmetrical property of the travel time characteristics along the observation line. As an indoor experiment system, 10 pairs of ultrasound transmitter/receiver are arrayed on a facing sides of the measurement region of 36 cm x 36 cm. Vortex wind fields generated by the electric fan (with diameter 190 mm) are reconstructed under the various wind source inclination conditions. By this means, precisions of the estimated vortex parameters (maximum vortex flow speed, size and position of the vortex wind field) are examined to justify the feasibility of the present method.

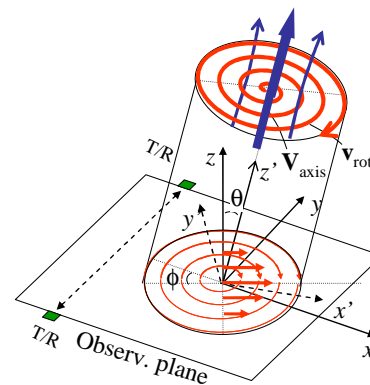


Figure 1. Schematic description of inclining vortex wind field.

2. ACOUSITC TOMOGRAPHY OF VORTEX WIND FIELDS

2.1 Model of inclining vortex wind field

We consider a model of up-flow inclining vortex wind field as follows. The wind field is assumed to be the sum of the vortex component \mathbf{v}_{rot} and axial flow component \mathbf{v}_{axis} in the inclined coordinate as

$$\mathbf{v} = \mathbf{v}_{rot} + \mathbf{v}_{axis} \quad (1)$$

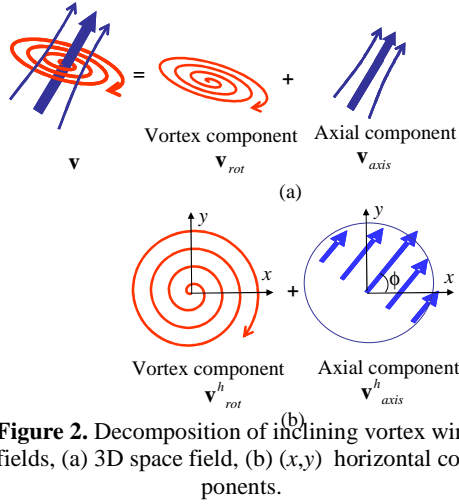


Figure 2. Decomposition of inclining vortex wind fields, (a) 3D space field, (b) (x,y) horizontal components.

We denote an observation coordinate (x,y,z) setting z axis to be normal to the (x,y) observation horizontal plane, as shown in Figure 1. We consider the tomographic problem to reconstruct the vortex wind flow field \mathbf{v}_{rot} from the observation of the bidirectional acoustic travel time difference data between facing pairs of transmitters and receivers. We define an inclining vortex wind field coordinate as (x',y',z') , where axial direction of the vortex is along z' axis, inclining angle between z' and z as θ , angle between x and projection of z' over the observation plane (x,y) as ϕ . We assume that the vortex wind fields component described by $\mathbf{v}_{rot}(x',y')$ is rotation symmetric around z' -axis, in addition, \mathbf{v}_{axis} is along z' -axis. For such case, model vortex field function is assigned as

$$\begin{cases} v_x' = -v_0 R \exp[-(R/R_w)^2] \sin \alpha \\ v_y' = v_0 R \exp[-(R/R_w)^2] \cos \alpha \\ v_z' = V_0 \exp[-(R/R_w)^2] \end{cases} \quad (2)$$

where v_0 and V_0 are amplitude coefficients of vortex and axial components, respectively, R_w is the width of vortex, (R,α) is a polar coordinate which is connected to the orthogonal coordinate (x',y') through the relation:

$$R = \sqrt{x'^2 + y'^2}, \quad \alpha = \tan^{-1}[y'/x'] \quad (3)$$

The relationship between (x,y,z) and (x',y',z') are given by the coordinate rotation formula, where observation coordinate (x,y,z) is transformed to the wind field coordinate (x',y',z') by rotating θ around y' -axis and then ϕ around z' -axis. Wind flow velocity in observation coordinate (v_x, v_y, v_z) is therefore related with that of the original coordinate (v_x', v_y', v_z') as

$$\begin{cases} v_x = -v_y' \sin \phi + \cos \phi (v_x' \cos \theta + V \sin \theta) \\ v_y = v_y' \cos \phi + \sin \phi (v_x' \cos \theta + V \sin \theta) \end{cases} \quad (4)$$

2.2 Description of inclining vortex wind fields with the travel time observation data

We consider the data observation arrangement where the acoustic wave transmitter and receiver facing pairs are placed on the opposite side along the observation line which is in parallel to x axis over the horizontal (x,y) plane. Bidirectional travel time difference $\Delta T(x)$ between facing pair elements is expressed with the use of the wind velocity field $\mathbf{v}^h(x,y)$ in the horizontal plane through the relation:

$$\Delta T = \frac{T_{ab} - T_{ba}}{2} \approx - \int_a^b \frac{\mathbf{v}^h(x,y) \cdot d\mathbf{l}}{c^2} \quad (5)$$

where T_{ab} is the travel time between transmitter a and receiver b , as well as T_{ba} between transmitter b and receiver a , $c(x,y)$ is sound velocity in the medium and $d\mathbf{l}$ is line element vector on the straight path between a and b .

We make a formulation for decomposing travel time difference $\Delta T(x)$ into the vortex component ΔT_{rot} and the axial flow component ΔT_{axis} like

$$\Delta T = \Delta T_{rot} + \Delta T_{axis} \quad (6)$$

From the equations (1),(5) and (6), horizontal (x,y) plane components of the vortex flow \mathbf{v}_{rot}^h is related with ΔT_{rot} as

$$\Delta T_{rot} = - \int_a^b \frac{\mathbf{v}_{rot}^h(x,y) \cdot d\mathbf{l}}{c^2} \quad (7)$$

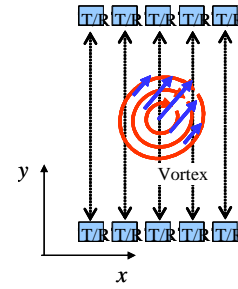


Figure 3. Acoustic wave transmitter and receiver arrangement for the vortex flow field imaging.

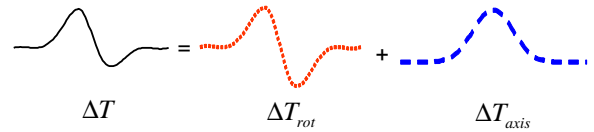


Figure 4. Decomposition of the travel time difference data into vortex and axial wind field component.

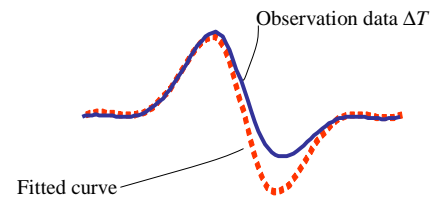


Figure 5. Estimation of the vortex travel time difference components by fitting the anti-symmetric theoretical curve.

2.3 Discrimination of vortex and axial flow component

It is noted here that ΔT_{rot} becomes anti-symmetric against the centre position of the vortex, on the other hand, ΔT_{axis} symmetric, using the assumption that vortex wind fields is rotation symmetric (see Figure.4). Applying the symmetric property of the travel time difference along the observation line, vortex flow components can be discriminated from the axial components. In particular, vortex field components ΔT_{rot} are estimated by fitting the anti-symmetric theoretical functional curve of eq.(2) to the observation data ΔT as shown in Figure

5. It is expected that ΔT_{rot} thus obtained is yielded by the vortex wind field components $\mathbf{v}_{rot}^h(x,y)$ in the horizontal (x,y) plane, similarly, ΔT_{axis} by the axial flow component by $\mathbf{v}_{axis}^h(x,y)$. Once ΔT_{rot} is obtained, the vortex wind field \mathbf{v}_{rot}^h can be reconstructed based on the method which is described in the next subsection.

2.4 Reconstruction of the vortex wind field

Knowing the vortex components of the travel time data as described above, the objective vortex wind field can be reconstructed based on the assumption that vortex wind fields is rotationally symmetric around the vertical axis. To this end, vortex flow \mathbf{v}_{rot}^h is represented by its vector potential Ψ^h . According to the assumption described before, vector potential of the vortex field must have only z' component. That is,

$$\mathbf{v}_{rot}^h = \nabla \times \Psi^h \mathbf{e}_z, \quad (8)$$

where \mathbf{e}_z denotes unit vector in axial z' direction.

With the substitution of (8) into (7), the vortex components of the travel time difference ΔT_{rot} is expressed as

$$\Delta T_{rot} = -\frac{1}{c^2} \int_a^b \nabla \times \Psi^h(x,y) \cdot d\mathbf{l}, \quad (9)$$

where Ψ^h is the vector potential of vortex flow \mathbf{v}_{rot}^h .

Equation (9) can be solved by applying the Fourier central slice theorem for the vector field, which is a straightforward extension of that for the conventional scalar field¹. To show this, we denote the parallel beam set of the travel time data as $\Delta T_\beta(\rho)$ along the coordinate ρ at rotational angle β . One-dimensional Fourier transform of travel time $\Delta T_\beta(\rho)$ with respect to ρ , which is denoted by $\tilde{T}_\beta(k)$, is then related to the two-dimensional Fourier transform of the vector potential:

$$\tilde{\Psi}(K_x, K_y) = -c_0^2 \frac{\tilde{T}_\beta(k)}{jk}, \quad (10)$$

where (K_x, K_y) is the spatial angular frequency of the vector potential field.

We assume here the vortex wind velocity field as rotationally symmetric. On this assumption, $\Delta T_\beta(\rho)$ becomes constant regardless to β . Therefore, data is obtained over the entire Fourier plane from a specified single rotational data $\Delta T_\beta(\rho)$. Vector potential $\Psi^h(x,y)$ is calculated by applying two-dimensional inverse Fourier transform of the data thus obtained. Finally, objective vortex wind velocity $\mathbf{v}_{rot}(x,y)$ can be obtained from the following rotation operation:

$$\mathbf{v}_{rot}^h(x,y) = \nabla \times \Psi^h(x,y) \quad (11)$$

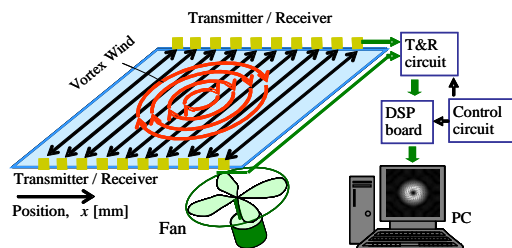


Figure 6. Indoor model system with multi-channel bidirectional ultrasonic transmitter receiver circuit.

3. EXPERIMENT EXAMINATION

3.1 Experiment Set-up

Figure 6 shows the indoor experimental set-up fabricated to examine the validity of the present vortex wind flow tomographic reconstruction method. To this end, 10 pairs of ultrasonic transmitter/receiver (with centre frequency 40kHz) were placed with spacing 40mm on the opposite sides of the square plane of 360mm x 360 mm. Sine pulse waves are sent from the transmitter and received waves transmitted through the measurement area were digitized by the digital signal processor (DSP). The measured travel data were transferred to the personal computer (PC) and wind flow tomography calculations were carried out. An electric fan with aperture diameter 190mm was placed underneath the horizontal measurement plane facing its front to obliquely upper direction with its inclination angle θ and rotation angle ϕ .

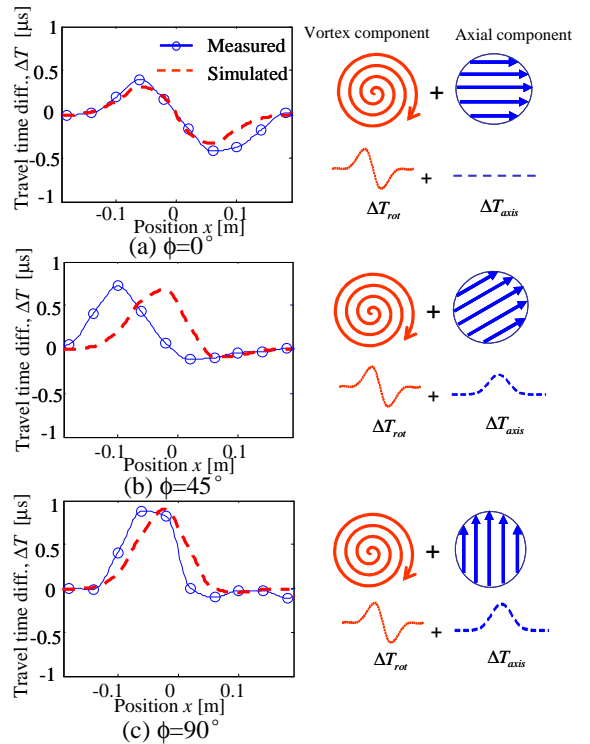


Figure 7. Variation of the travel time difference along x -axis. Left-hand figures show the results for the different inclination angles: (a) $\phi=0^\circ$, (b) $\phi=45^\circ$, (c) $\phi=90^\circ$. The marked solid lines and the broken lines show the measured and simulated results, respectively. Right-hand figures show the schematic explanation of the dependencies for each result.

3.2 Measured travel time data along x -axis for the different vortex inclination angles

Inclination angle of wind fan axis was set at $\theta=30^\circ$, and its rotation angle ϕ was changed at $\phi=0, 45, 90^\circ$. Figure 7 shows the variation of the travel time difference $\Delta T(x)$ along observation x -axis. The solid lines are measured results and dotted lines results of the simulation, where (a) shows the case for $\phi=0^\circ$, (b) for $\phi=45^\circ$, and (c) for $\phi=90^\circ$, respectively. Note that the simulations were carried out under the same condition used in the experiment except that the centre position of the vortex was set at the origin.

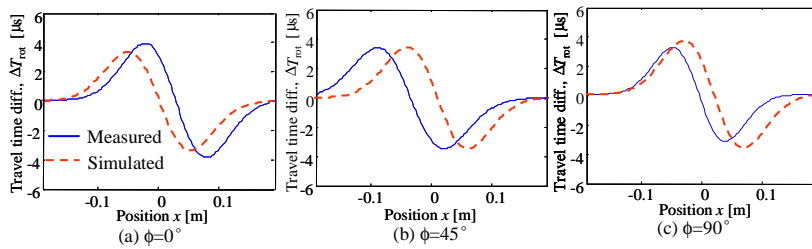


Figure 8. Extracted vortex field components from the travel time data of Figure 7 for different observation angle (a) $\phi=0^\circ$, (b) $\phi=45^\circ$, (c) $\phi=90^\circ$.

Except for this point, we can see that the measured results are in good agreement with the theoretical anticipations. As explained with the illustrations in the right-hand side of Figure 7, travel time variation along x -axis shows symmetric in Figure (a), on the other hand, it approaches asymmetric variation in Figures (b) and (c). The results are due to the fact that travel time differences caused by the symmetric axial flow component becomes dominant compared to the ones by the anti-symmetric vortex flow as the rotation angle ϕ approaches to 90° .

3.3 Results of the vortex wind field profile reconstruction

Next, model theoretical function was fitted to the travel time difference data of Figure 7. The extracted vortex field components ΔT_{vor} were shown in Figure 8, where solid lines and dotted lines correspond to the measured and simulated results, respectively. Finally, using the extracted data, vortex velocity fields were reconstructed. Figure 9 shows an example of experimentally obtained wind flow vector image for the case when $\phi=0^\circ$. Furthermore, for the quantitative evaluation, Figure 10 shows the maximum wind velocity and width of the reconstructed vortex fields, where the results were compared between the experiment (circles) and the simulation (solid line). We can see that the measured results were relatively good agreement with the simulated ones regardless of the rotation angles.

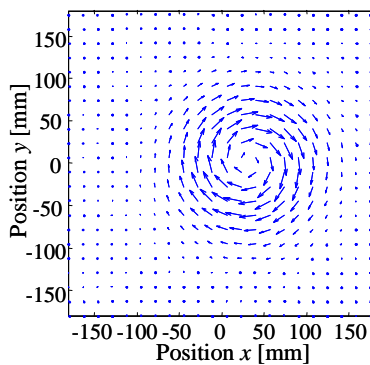


Figure 9. Experimentally reconstructed vortex velocity field image generated by the inclining vortex wind source for the inclination angle $\theta=30^\circ$ and rotation angle $\phi=0^\circ$.

4. CONCLUSIONS

An image reconstruction method of the inclining vortex air flow profile by acoustic tomography has been demonstrated, having capability of estimation of vortex flow discriminating from vertical axial flow. As a result of the examination ex-

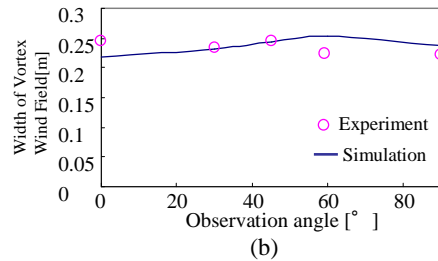
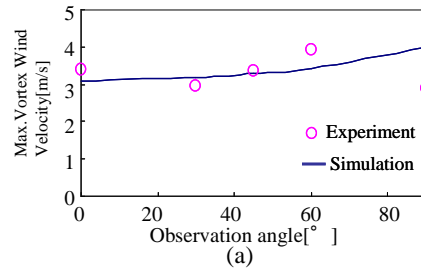


Figure 10. Reconstructed values of the vortex fields : (a) maximum wind velocity, (b)width of the vortex. Measured and simulated values are shown with circles and solid lines, respectively.

periment, it was demonstrated that the vortex wind velocity fields could be reconstructed with satisfactory quantitative precision of the vortex maximum velocities and size, to justify the feasibility of the present method in actual strong wind monitoring applications.

REFERENCES

1. S. J. Norton, "Tomographic reconstruction of 2-D vector field: application of flow imaging", *Geophys.J.* 97, pp.161-168(1988).
2. M. N. Rychagov and H. Ermert, "Applicability of wave tomography methods for 2-D imaging", *IEEE Ultrasonics Symp.*, pp.1731-1975 (1994).
3. P. Beckord, G. Ho'felmann, H. O. Luck, and D. Franken, "Temperature and velocity flow fields measurements using ultrasonic computer tomography", *Heat MassTransfer*, 33, pp. 395-403 (1998) .
4. T. H. Gan, D. A. Hutchins, P. W. Carpenter, and W. M. Wright, "Simultaneous reconstruction of flow and temperature cross-sections in gases using acoustic tomography", *J. Acoust. Soc. Am.*, 114, pp. 759-766 (2003).
5. H.Li and A.Yamada,"Imaging of time and space variation of vortex wind velocity fields using acoustic tomography", *Jpn.J.Appl.Phys.*, 47, pp.3940-3945 (2008).
6. H. Li, T. Ueki, K. Hayashi, and A. Yamada," High-speed vortex wind velocity imaging by acoustic tomography", *Acoustical Imaging*, 29, pp.347-352(2008).